Journal of Fluids and Structures 18 (2003) 271–285

JOURNAL OF FLUIDS AND STRUCTURES

www.elsevier.nl/locate/jnlabr/yjfls

Steady flow past a vertical surface-piercing circular cylinder

J.R. Chaplin[a,*], P. Teigen[b]

[a] *Department of Civil and Environmental Engineering, University of Southampton, Southampton SO17 1BJ, UK*
[b] *Statoil Research Centre, Postuttak, Trondheim N-7005, Norway*

Received 15 July 2002; accepted 15 July 2003

Abstract

This paper describes experiments in which a vertical surface-piercing circular cylinder with a large draught was towed at steady speeds through water initially at rest. The cylinder diameter d was 210 mm, and measurements were made of pressures around its circumference at elevations between $2.4d$ below still water level to $0.7d$ above, at Froude numbers (based on d) up to 1.67. The tests were carried out at a constant ratio of Reynolds number to Froude number of 2.79×10^5. The total resistance coefficient reached a maximum at a Froude number of about 1, when that part of the loading that can be attributed to the presence of the free surface was equivalent to the submerged form drag on a length of cylinder of about $0.9d$. Measurements are also presented of the run-up on the front of the cylinder and of the depth of the depression at the back. Previous measurements by Hay (Flow about Semi-submerged Cylinders of Finite Length. Princeton University Report, Princeton, NJ, 1947) for the case of a cylinder with a submerged free end, and by Hsieh (Proc. Am. Soc. Civil Eng. 90 (1964) 161) of forces on cylinders standing on the floor of an open channel, are reanalysed. In most respects these results are found to be compatible with the present data for a cylinder of large draught.

1. Introduction

The flow past a vertical cylindrical body that extends through the free surface in a steady stream is a familiar and fascinating sight. Well-known annotated drawings by Leonardo da Vinci show the standing waves that are produced by the body, and the 'braided' nature of the motion at the surface in its wake. But there seem to have been few measurements in the region close to the surface in this flow, probably because it differs significantly from the more obviously important case of a streamlined body of shallow draught in forward motion. Also, in many engineering applications where bluff bodies (for example, bridge piers) do intersect a free surface, the evidence suggests that the particular features of the surface are often not very important.

Nevertheless, this complicated flow has the intrinsic appeal of geometric simplicity, and, if the effects of finite draught and surface tension effects are neglected, of having just two defining parameters: a Froude number $\mathrm{Fr} = V/\sqrt{gd}$ (where V is the velocity of the current and d the diameter of the cylinder) and a Reynolds number $\mathrm{Re} = Vd/\nu$. For this reason, it is an ideal test case for those research groups which are developing numerical solutions for free surface flows in the presence of viscosity (e.g., Yeung and Yu, 2001). Also, in some cases, for example that of the columns of a Tension Leg Platform in a current (Younis et al., 2001) where the Froude number is small, it seems reasonable to assume that the free surface may be treated as a plane boundary with zero shear stress, or in other words represented as a plane of symmetry. But in reality, at appreciable Froude numbers, it is not clear how the surface affects the separated flow beneath, and whether the pressure distribution around the cylinder at large submergences is significantly changed by the presence of

*Corresponding author. Tel.: +44-23-8059-2843; fax: +44-23-8067-7519.
E-mail addresses: j.r.chaplin@soton.ac.uk (J.R. Chaplin), pte@statoil.com (P. Teigen).

0889-9746/$ - see front matter © 2003 Elsevier Ltd. All rights reserved.
doi:10.1016/j.jfluidstructs.2003.07.009

the free surface above. The fact that the drag on a cylinder of finite length in a steady uniform stream is influenced over very large axial distances by the existence of a free end (Goldstein, 1965) shows how sensitive the separated flow can be to out-of-plane disturbances.

This paper describes measurements of pressures around a vertical surface-piercing circular cylinder in steady currents with Froude numbers up to 1.67 and Reynolds numbers up to 4.7×10^5. It is convenient to carry out such experiments at constant values of the ratio $\mathrm{Re}/\mathrm{Fr} = \sqrt{gd^3}/\nu$, since this is determined just by the diameter of the cylinder and the temperature of the water. Section 2 reviews previous experimental investigations and reanalyses measurements by Hay (1947) and Hsieh (1964) to reveal some measure of agreement. Section 3 describes the arrangements for the present experiments, and the results are discussed and compared with earlier data in Section 4.

The loading on the cylinder is clearly associated both with flow separation and wavemaking, but it is not possible to identify corresponding distinct components of the force because these features are strongly inter-related. One possible approach is to consider the total force to be the sum of the ideal fluid wavemaking resistance, discussed in Section 2, and a second part that is assumed to be predominantly due to viscosity. Another is to identify the force that would act on the cylinder at the same Reynolds number in the absence of the free surface, and to consider the rest to be mainly due to the generation of waves. Both are discussed below in the light of the available measurements. Following the second approach, the total force $F(L)$ acting on a cylinder of infinite draught down to an elevation L beneath the still water level is split into components of viscous drag F_D and surface resistance F_S. The former is defined by

$$F_D = C_{d0}\frac{1}{2}\rho V^2\, d\, L, \tag{1}$$

where C_{d0} is the sectional force coefficient observed in the absence of the free surface at the same Reynolds number. A surface resistance coefficient is defined by

$$F_S = F - F_D = C_S\frac{1}{2}\rho V^2 d^2 \tag{2}$$

and

$$F = C_R\frac{1}{2}\rho V^2\, d\, L \tag{3}$$

defines a total resistance coefficient C_R The sectional force coefficient C_d is a function of elevation z (measured relative to still water level), and

$$\int_{-L}^{\eta} C_d\, \mathrm{d}z = C_R L, \tag{4}$$

where η is the elevation of the maximum run-up on the cylinder.

2. Previous work

This section reviews data obtained in experiments by Hay (1947) for apparently military applications, by Hsieh (1964), who was concerned with the loading on bridge piers, and by Hogben (1974), who inferred estimates for wave resistance from measurements of the wave pattern behind a towed vertical cylinder. Some velocity measurements around a vertical surface-piercing cylinder were reported by Inoue et al. (1993). Hogben speculated that the surface resistance of a cylinder could be estimated by assuming that the fluid motion could be modelled by the potential flow around a vertical surface-piercing elliptical cylinder chosen to represent the outline of the circular cylinder and its near wake. It is therefore helpful to mention first the theory for wave resistance of a vertical surface-piercing cylinder in the absence of viscosity.

2.1. The ideal fluid wave resistance

Kotik and Morgan (1969) discussed the inviscid flow past vertical surface-piercing cylinders of elliptical cross-sections and infinite draught in a steady current. They identified several singularity distributions that satisfied the kinematic condition on the body and the linearized free surface boundary condition, but showed that there was not a unique result for the wave resistance. On pragmatic grounds they were in favour of that obtained from surface source distributions, and Hogben (1974) came to the same conclusion. Using this approach, Kotik and Morgan's formula for the wave resistance coefficient of a cylinder of elliptical cross-section with semi-diameters a in the flow direction and b in

the transverse direction is

$$C_S(\mathrm{Fr},\varepsilon) = 2\pi(1+\varepsilon)^2 \int_1^\infty \frac{J_1^2(\lambda\Omega/2\varepsilon\mathrm{Fr}^2)}{\lambda^2\Omega^2\sqrt{\lambda^2-1}}\,\mathrm{d}\lambda, \tag{5}$$

in which $\varepsilon = b/a$, $\Omega = \sqrt{1+(\lambda^2-1)\varepsilon^2}$, and Fr and C_S are defined as above but with d replaced by the width of the ellipse $2b$. Not surprisingly, the wave resistance calculated in this way is greater than that obtained from Michell's integral (see Newman, 1977, p. 282), which neglects the fullness of the body, though they converge as $\varepsilon \to 0$. The result from Eq. (5) for a circular cylinder $\varepsilon = 1$ is shown as a continuous line in Fig. 1. (Also plotted is that for $\varepsilon = 0.2$, in a way that illustrates Hogben's approximation $C_S(\mathrm{Fr},\varepsilon) \approx \varepsilon^{0.4} C_S(\varepsilon^{1/2}\mathrm{Fr}, 1)$.) For a circular cylinder, C_S reaches a maximum of 4.71 at $\mathrm{Fr} = 0.58$, and falls to less than 1% of this for $\mathrm{Fr} > 3$. Fig. 1 also shows the wave resistance coefficient for an elliptical cylinder of infinite draught obtained from Michell's integral, a function only of $\varepsilon^{1/2}\mathrm{Fr}$.

2.2. Measurements by Hay (1947)

In Hay's experiments, vertical surface-piercing cylinders of various diameters and draughts were towed in turn along a channel 1.37 m wide containing water to a maximum depth of 1.2 m. The free bottom end of each test cylinder (with no endplate) was well above the floor of the tank, and its submerged length was changed by adjusting either its elevation on the towing carriage, or the water level. There were seven cylinders (of diameters 3.2, 6.4, 12.7, 25.4, 50.8, 101.6 and

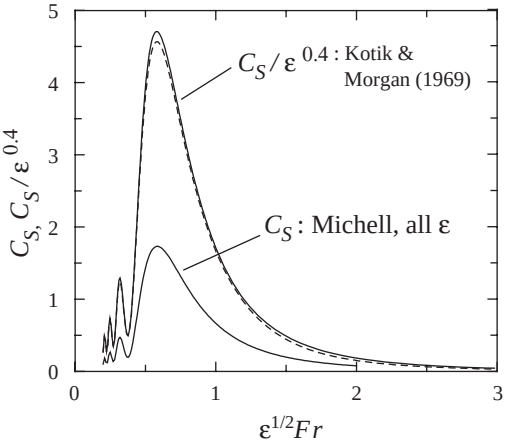

Fig. 1. Wave resistance coefficient C_S for vertical cylinders of elliptical cross-section of ellipticity ε and infinite draught, in ideal fluid flow. Results of Kotik and Morgan's (1969) solution based on a distribution of sources over the cylinder surface are shown for $\varepsilon = 1$ (continuous line) and $\varepsilon = 0.2$ (dashed line).

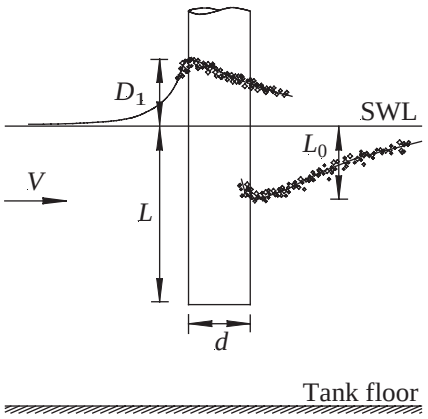

Fig. 2. Definition sketch for Hay's (1947) experiments.

203.2 mm) and most were tested at each of six submergences between 1 and 32 diameters (again in ratios of powers of 2). In each case a large volume of data were collected on total mean resistance and mean water surface elevations, and much of it is tabulated. Hay's report also contains many remarkable photographs showing the surface motion and the spray generated by the cylinder at Froude numbers Fr up to about 28. Since these measurements are rather inaccessible, and for the most part were not presented in the most revealing way or discussed very thoroughly, some of the data have been reprocessed and reanalysed here.

Fig. 2 is a definition sketch for Hay's experiments, showing the extent D_1 of the run-up on the centre-line at the front of the cylinder, and of the depression L_0 of the maximum drawdown on the centre-line at the rear. These displacements, averaged over the duration of each run at constant speed and normalized with respect to the cylinder diameter d, are plotted in Figs. 3 and 4 for each cylinder, identified by the corresponding value of Re/Fr. In the experiments the water temperature varied (unaccountably) between 14°C and 24°C, and for present purposes mean values of viscosity have been taken for all the tests with each cylinder.

In each plot in Fig. 3, a continuous line represents the implication of Bernoulli's equation, $D_1/d = \mathrm{Fr}^2/2$, that the maximum run-up is exactly that which would be supported by the stagnation pressure. This is valid for inviscid flow and, in practice, likely to be appropriate at high Reynolds numbers and low Froude numbers. Also shown (as a broken line) is a power law $D_1/d \propto \mathrm{Fr}^B$ fitted to the data over the range of Froude numbers (starting from the lowest) for which this form seems appropriate. As can be seen from the values of B in Table 1, the maximum observed run-up is almost proportional to the Froude number at low Reynolds numbers, but the relationship becomes progressively closer to a quadratic one as Re/Fr is increased. For the high Reynolds number cases, where the maximum run-up D_1/d is close to

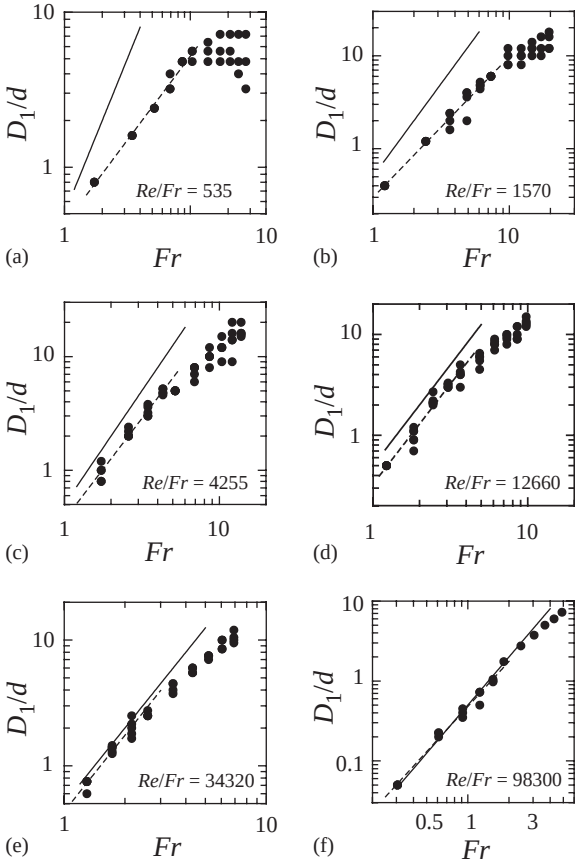

Fig. 3. Hay's (1947) measurements of the maximum run-up on the front face of the cylinder as a function of Froude number for all L/d. A continuous line in each case represents Bernoulli's equation $D_1/d = \mathrm{Fr}^2/2$. Dashed lines are power laws of the form $D_1/d = A\mathrm{Fr}^B$ fitted to the data. The powers B, and the Froude numbers Fr_c that correspond approximately to the upper limit of the validity of this relationship are set out in Table 1.

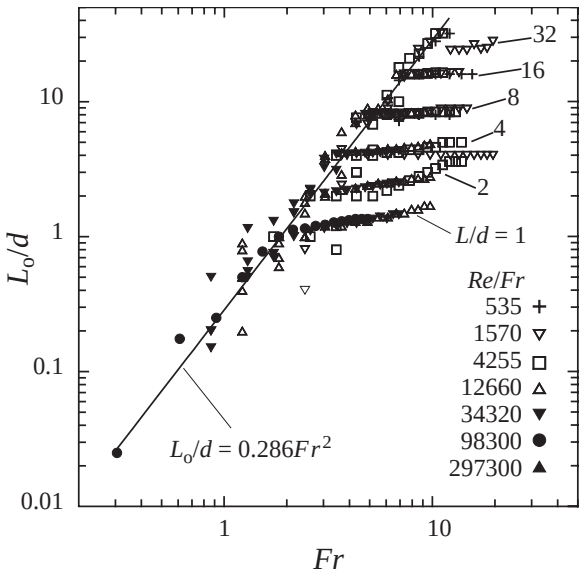

Fig. 4. Hay's (1947) measurements of the depth L_0 of the depression on the centre-line behind the cylinder, normalized with respect to the cylinder's diameter d, plotted as a function of the Froude number. The line is a best-fit quadratic to the data for cases where $L_0 < L$.

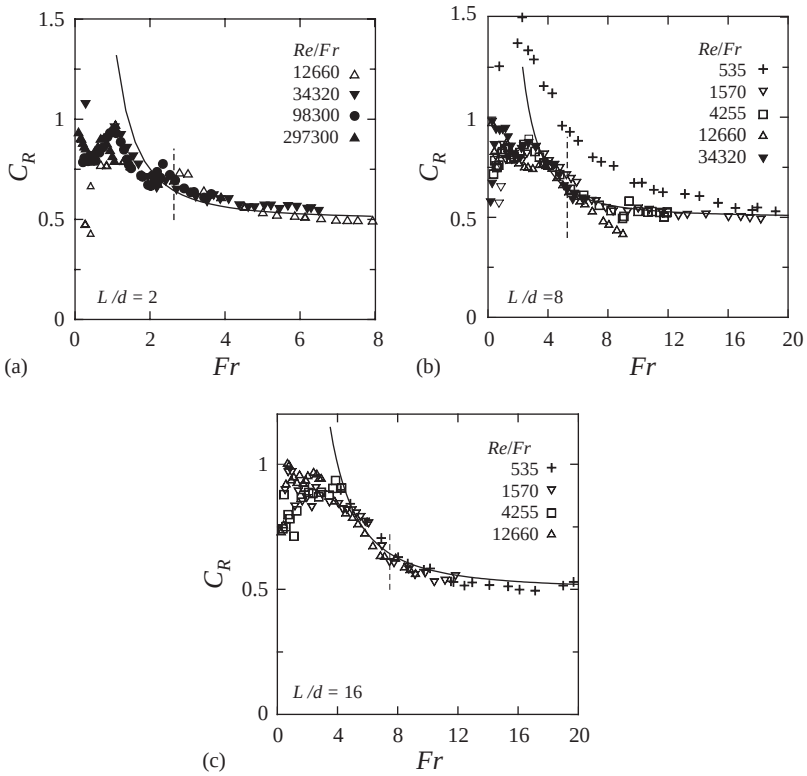

Fig. 5. Total resistance coefficients from Hay (1947) for: (a) $L/d = 1$, (b) $L/d = 8$, and (c) $L/d = 16$. Vertical dashed lines indicate Froude numbers corresponding to the onset of the fully ventilated condition, based on data of Fig. 4. Continuous lines in (a–c) are $C_R = \frac{1}{2}(1 + 1/\mathrm{Fr}_L^2)$.

Table 1
Coefficients B in power laws $D_1/d \propto \mathrm{Fr}^B$ fitted to Hay's (1947) measurements of the initial maximum run-up on the front face of the cylinder shown in Fig. 3

Cylinder diameter (mm)	Re/Fr	B	Fr_c
3.2	535	1.1	11
6.4	1570	1.5	8.3
12.7	4255	1.8	4.8
25.4	12660	2.0	4.1
50.8	34320	2.0	2.9
101.6	98300	1.9	2.1

At higher Froude numbers, $\mathrm{Fr} > \mathrm{Fr}_c$, the data departed from this relationship.

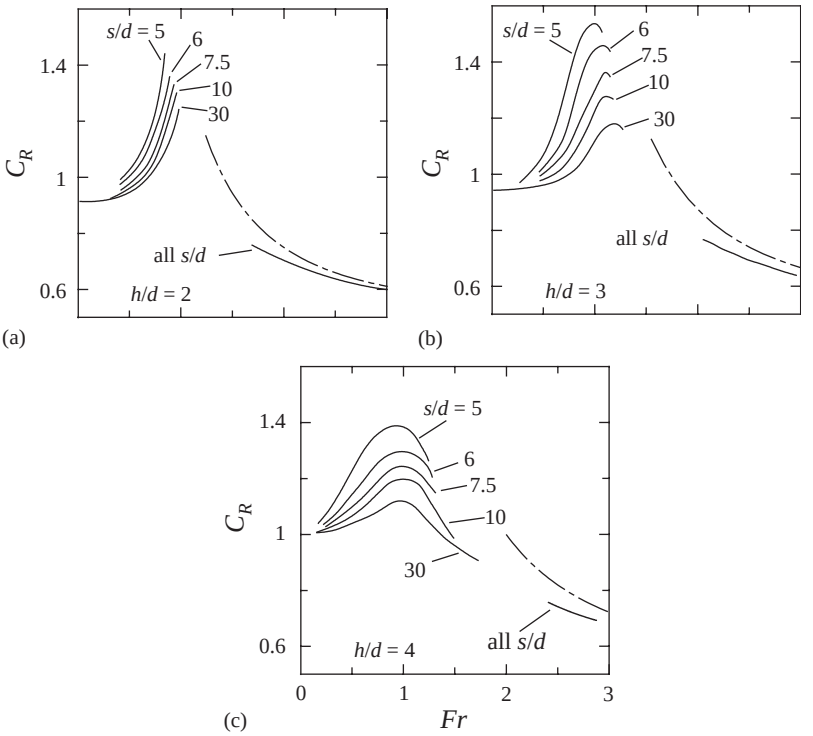

Fig. 6. Curves fitted to measurements by Hsieh (1964) of the total resistance of a surface-piercing cylinder of diameter d in an array with spacing s across a channel with flow of depth h. Broken lines are $C_R = \frac{1}{2}[1 + (h/d)/\mathrm{Fr}^2]$.

$\mathrm{Fr}^2/2$ in accordance with Bernoulli's equation, it follows that the pressure variation on the wetted front face of the cylinder will be approximately hydrostatic.

The run-up measurements break away from a power law at a Froude number that can be identified quite clearly in most cases, and is denoted Fr_c in Table 1. It is not clear from Hay's photographs what changes take place in the flow at Fr_c, but it is noticeable that at higher Froude numbers the maximum elevation of the vertical sheets of water behind the cylinder was greater than that recorded as D_1.

Hay's measurements of the maximum depression L_0 of the water surface behind the cylinder, normalized with respect to the cylinder's diameter, are plotted in Fig. 4. As the Froude number was increased, the depression became deeper until it reached the elevation of the bottom of the cylinder, when the whole of the rear face was ventilated. When the Froude number was increased further, in cases where the bottom of the cylinder was not deeply submerged, the depression of the water surface reached a still lower level some distance downstream from the rear of the cylinder.

The line $L_0/d = 0.286\,\mathrm{Fr}^2$ (equivalent to $V/\sqrt{gL_0} = 1.87$) in Fig. 4 is the best quadratic fit to the maximum measured water surface depression for all cases with $L_0 < L$, when the ventilated region did not extend to the bottom of the cylinder. If the elevation of the water surface on the rear face of the cylinder were determined simply by the base

pressure at lower levels, this would imply a base pressure coefficient of $C_{pb} = -0.57$. Comparable values reported in Zdravkovich (1997, p. 132) for a circular cylinder in a uniform incident flow at similar Reynolds numbers are in the range $-1.2 < C_{pb} < -0.7$. The difference can probably be attributed to the fact that Hay's cylinders had a free end (a situation in which, in a uniform incident flow, Farivar (1981) measured considerably higher base pressure coefficients), and to the bubbly nature of the flow near the surface.

Resistance coefficients obtained by Hay are plotted in Fig. 5 for three submergence ratios, $L/d = 2$, 8 and 16. All of Hay's results for these cases are plotted here, except for some runs at the lowest speeds (when the data are rather noisy), and others at a water temperature of 14°C, for which resistance coefficients improbably jumped by about 50% at Froude numbers around 12. In other respects the results of similar tests at different water temperatures are as consistent as can be expected, bearing in mind the small difference in Reynolds numbers. A vertical dashed line in each plot in Fig. 5 indicates the Froude number which, according to the data in Fig. 4, corresponds to the onset of the fully ventilated condition at $\mathrm{Fr}_L = 1.87$, where $\mathrm{Fr}_L = V/\sqrt{gL}$ is the Froude number based on the cylinder's draught.

2.3. Measurements by Hsieh (1964)

Hsieh measured the resistance of one of a row of model cylindrical bridge piers of 25.4 mm diameter placed across the width of a laboratory open channel for depth ratios h/d between 2, 3 and 4, where h is the depth of the incident flow. The separation s between centres of adjacent piers was such that $5 < s/d < 30$ and $\mathrm{Re}/\mathrm{Fr} \approx 11100$. No data are given on the velocity profile of the incident stream, and it is inevitable that the flow around the piers and the forces on them would have been influenced by the presence of the boundary layer in the channel.

The results were presented in the form of the total resistance coefficient C_R plotted against the Froude number $V/\sqrt{gh}$. Because of the instability of critical flow in an open channel, measurements could not be made close to $V/\sqrt{gh} = 1$, but Hsieh covered a sufficient range of speeds at depth ratios of 3 and 4 to reveal maxima in the resistance coefficients at about $\mathrm{Fr} = 1$. Curves fitted through the results are plotted in Fig. 6.

2.4. Measurements by Hogben (1974)

Hogben (1974) carried out experiments with a cylinder of diameter 0.316 m and draught 1.22 m (without an endplate), at Froude numbers up to about 1.2. The surface resistance was estimated from downstream measurements of water surface elevations (Hogben and Standing, 1975), neglecting the effects of the overturning of the water surface that must have occurred. It was claimed that the results showed some similarity with Kotik and Morgan's (1969) theory (Eq. (5)) with $\varepsilon = 0.2$. However, this seems to be the case only if a factor of ε^{-2} has been omitted in the calculation of the data in Hogben's Fig. 3. After multiplying these results by 25, therefore, the corresponding values of C_S from Hogben (1974) are compared with the present measurements in Section 4.

2.5. Concluding remarks

Anticipated forms of the pressure distributions on the centre-lines of the front and rear faces of the surface-piercing cylinder are sketched in Fig. 7. (For later reference, the outer sketches at (a) and (d) show the corresponding pressures that would be recorded by transducers on the cylinder, if they had been zeroed in still water. It is worth noting that in the ventilated region the pressures recorded in this way on the rear of the cylinder would fall from zero with a negative hydrostatic gradient.)

Fig. 7 also provides a basis for a simple estimate of the total resistance coefficient C_R at high Reynolds numbers. Firstly, at low Froude numbers, in the region $-L_0 < z < V^2/2g$ the rear of the cylinder is exposed to the atmosphere, while the relative pressure on the front increases linearly from zero at $z = V^2/2g$, to $\frac{1}{2}\rho V^2 + L_0\rho g$ at $z = -L_0$. If this pressure difference were to act over the projected frontal area of the cylinder it would result in a contribution to the resistance coefficient of

$$\Delta C_R = \frac{\mathrm{Fr}^2}{(L/d)} \left[\frac{1}{2} + \frac{(L_0/d)}{\mathrm{Fr}^2}\right]^2. \tag{6}$$

Furthermore, if the loading on the submerged part of the cylinder in these conditions were characterized by a drag coefficient C_{d0}, this would create a second contribution to the resistance coefficient of $C_{d0}(1 - L_0/L)$. The total, substituting $L_0/d = 0.286\ \mathrm{Fr}^2$ from above, amounts to

$$C_R = C_{d0} + \frac{Fr^2}{(L/d)}\,(0.618 - 0.286\ C_{d0}). \tag{7}$$

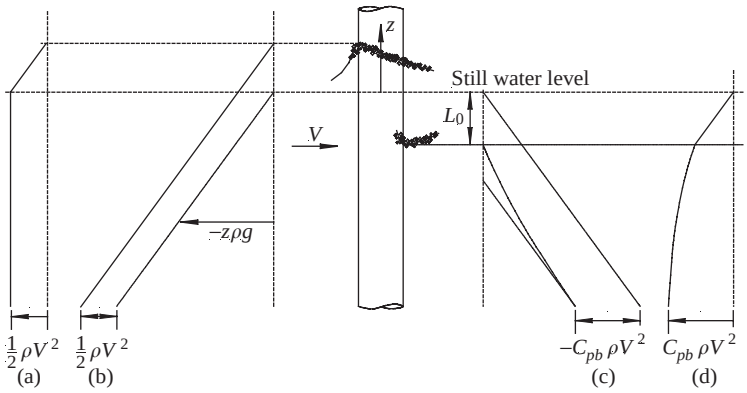

Fig. 7. Sketches of pressure distributions on the upstream (left) and downstream (right) faces of the cylinder. Continuous lines at (b) and (c) show total pressures relative to the atmospheric pressure datums represented as dashed vertical lines. Those at (a) and (d) are the corresponding distributions that would be recorded by pressure sensors that had been zeroed in still water conditions. Note that those at (d) would be recorded as negative pressures at all points.

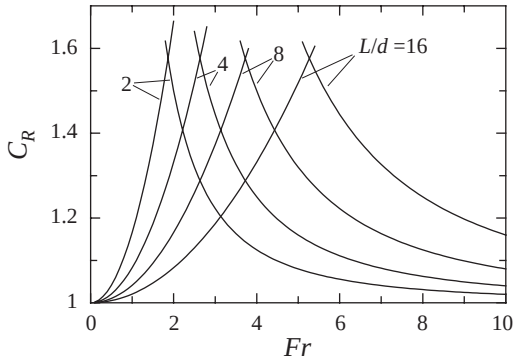

Fig. 8. Empirical formulae for the total resistance coefficient C_R as functions of the Froude number. Those on the left are from Eq. (7) with $C_{d0} = 1$; those on the right from Eq. (8).

Secondly, at high Froude numbers, the entire rear face of the cylinder is ventilated, and (as is shown by pressure measurements presented below) the run-up on the front no longer exerts hydrostatic pressure over the region $0 < z < V^2/2g$. This is probably because the flow there is bubbly and not everywhere in contact with the cylinder. Under these conditions the mean pressure difference between the centre-lines of the upstream and downstream faces of the cylinder can be seen to be $\frac{1}{2}\rho V^2 + \frac{1}{2}L\rho g$ (a form proposed by Hoerner, 1956, pp. 10–15) in the region $-L < z < 0$. If this pressure difference were to act on the projected frontal area L/d, the corresponding resistance coefficient would be

$$C_R = 1 + \frac{(L/d)}{\mathrm{Fr}^2}. \tag{8}$$

Eqs (7) and (8) are plotted in Fig. 8 for various L/d values. They overestimate the values of C_R obtained by Hay and Hsieh because the mean pressure differences between the front and back of the cylinder will be substantially less than those assumed above for the centre-lines. But some features of the dependence of C_R on Fr are similar to those observed in the measurements. As in Hay's data there is a maximum in C_R at a Froude number which increases with L/d. And if the right-hand side of Eq. (8) is multiplied by an empirical factor of 0.5, the result agrees quite well with Hay's and Hsieh's measurements for all except the lowest range of Reynolds numbers. This is true not only for fully ventilated cases $\mathrm{Fr}_L > 1.87$, but also at somewhat lower Froude numbers, as is shown in Figs. 5 and 6.

The experiments described in the next section were undertaken to complement these results with more detailed measurements at Froude numbers less than 2.

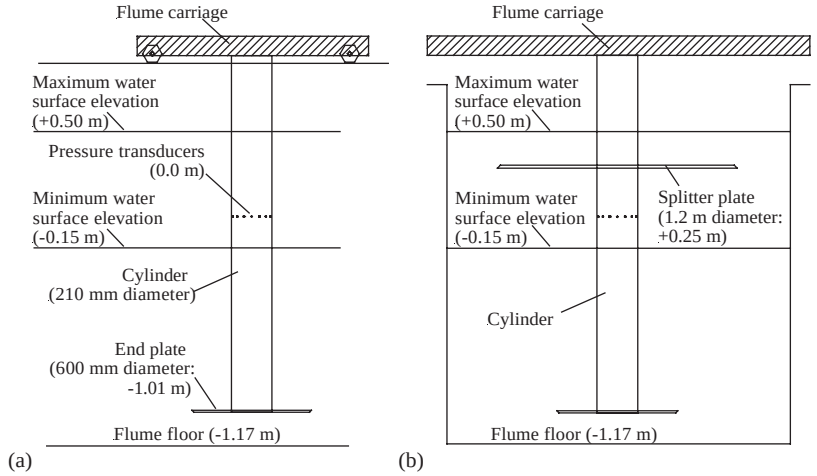

Fig. 9. Sketches of (a) the side view and (b) the cross-section of the cylinder mounted on the flume carriage. Elevations are shown relative to the pressure transducers. The splitter plate shown in (b) was used only during initial tests, to minimize the effect of the free surface on the measurements.

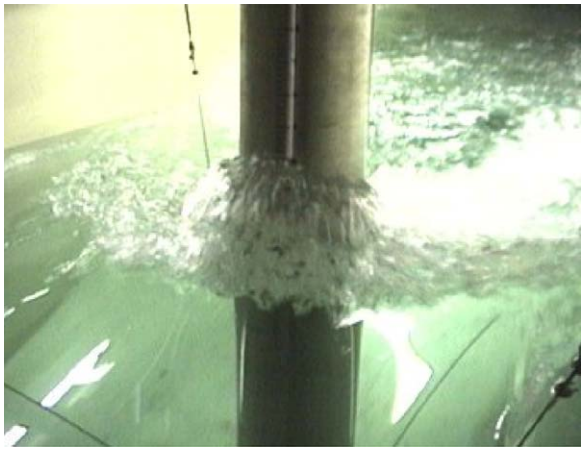

Fig. 10. Flow upstream of the cylinder towed at Froude number Fr = 1.64.

3. Experimental arrangements

The experiments were carried out at $Re/Fr = 2.79 \times 10^5$ with a smooth stainless-steel cylinder of 210 mm diameter, equipped at one section with a ring of 16 flush mounted pressure transducers equally spaced around its circumference. The cylinder was mounted vertically, as shown in Fig. 9, beneath the carriage of the 55 m flume at City University, London. This flume was 1.75 m wide and could be filled to any depth up to 1.75 m. The ring of pressure transducers was at an elevation of 1.17 m above the floor of the flume, and in repeated tests with different water levels, was between 450 mm below the still water surface ($z/d = -2.38$), and 150 mm above it ($z/d = 0.71$). The lower end of the cylinder passed over the floor of the flume with a few centimetres to spare, and was fitted with a 600 mm diameter endplate. It seems reasonable to assume that at a minimum submergence of almost five diameters, the bottom of the cylinder was too deep to have a significant effect at the free surface. A splitter plate of 1.2 m diameter (shown in Fig. 9(b)) was attached to the upper part of the cylinder for some tests, as mentioned below. The pressure datum for each transducer was that measured with the cylinder stationary in still water before the start of the run.

Results presented below were derived from measurements made under steady conditions, while the cylinder was towed along the flume at constant speeds in the range 0.6–2.4 m/s, corresponding to Reynolds numbers Re between 1.2×10^5 and 4.6×10^5, and Froude numbers Fr from 0.4 to 1.7. The output signals from the pressure transducers, and the carriage speed, were sampled at 100 Hz. Fig. 10 shows the cylinder being towed at Fr = 1.64.

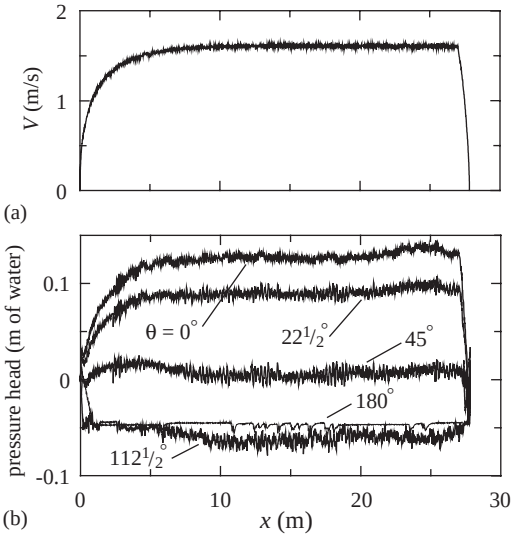

Fig. 11. Examples of recordings of (a) the velocity of the carriage and (b) simultaneous pressure measurements at five positions around the cylinder, measured from the upstream stagnation point. The pressure transducers were 50 mm below still water level.

Typical unfiltered pressure records are shown in Fig. 11 for a case in which the water surface was 50 mm above the ring of pressure transducers, and the target towing speed was 1.6 m/s (Fr = 1.11). Pressures are shown at five points around the cylinder, measured by the angle θ from the upstream stagnation point, and are plotted against distance x along the tank from the point at which the test was started. In this case the carriage speed became steady after the first 10 m, and, except for high-frequency oscillations at the cylinder natural frequency of about 4 Hz, the pressures were then almost constant. There was no clear evidence of vortex shedding in this or any other case. In Fig. 11, a Strouhal number of 0.2 would correspond to a frequency of about 1.5 Hz, and a spatial period of about 1 m. Towards the end of the run (from about $x = 20$ m in Fig. 11) there was typically a slight increase in pressure, due to a rise in the water level caused by a wave that had been reflected from the end of the tank. The time of arrival of this wave at the cylinder could be estimated quite accurately by assuming that it travelled from the cylinder initial position at the start of the test, with the shallow water wave speed of $\sqrt{gh}$, where h is the water depth. Results discussed below were derived from the mean pressures measured around the cylinder over a time interval that began when the cylinder had been travelling about 10 diameters after reaching a constant speed (at a distance of between 4 and 12 m from the start of the run), and ended shortly before it encountered the reflected wave.

Pressures are plotted in Fig. 11 as heads of water, and zero represents a head of 0.05 m (the initial submergence of the transducers) above atmospheric. In the ventilated region over the rear quadrant of the cylinder under tow, the measured head is, as expected, close to -0.05 m, except when splashes of water impacted on the transducers.

4. Discussion of results

4.1. Drag and resistance coefficients

The experiments were done in a particularly Reynolds number-sensitive regime, and so initial tests were carried out to check whether, when free surface effects were eliminated as far as possible, the measured drag coefficients agreed with definitive results for a smooth cylinder at the same Reynolds numbers. For these tests, the 1.2 m (5.7d) diameter splitter plate was fitted to the cylinder at a section 250 mm (1.2d) above the pressure transducers, and the tank was filled to its maximum level, with the still water surface 250 mm above the splitter plate. This arrangement is shown in the cross-section sketched in Fig. 9(b). Sectional drag coefficients obtained by numerical integration of the pressures around the cylinder are plotted in Fig. 12, and are in reasonable agreement with published data for uniform incident flow past a smooth cylinder at the same Reynolds numbers. The differences are characteristic of the effects of a small degree of surface roughness, and were probably generated by a slight vibration of the cylinder on the carriage.

For the remainder of the tests the splitter plate was removed, and measurements were made over a range of speeds at each of 12 water depths. Sectional force coefficients are plotted against the elevation z/d in Fig. 13, where each set of

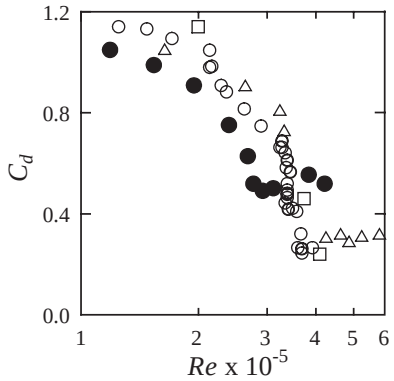

Fig. 12. Solid symbols show drag coefficients obtained from pressure measurements at a deeply submerged section with the splitter plate in position. The remaining symbols are data from sources similarly identified in Zdravkovich (1997, Fig. 6.6) for the drag on a smooth cylinder in uniform steady flow.

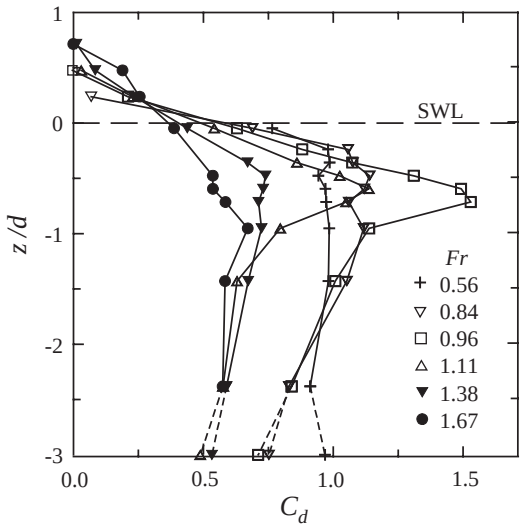

Fig. 13. Drag coefficients as functions of elevation at various Froude numbers. Those obtained for $z/d = -2.38$ in the presence of the splitter plate (plotted in Fig. 12) are shown at $z/d = -3$. They are joined by broken lines to the results for the same section measured without the splitter plate.

data are identified by the corresponding Froude number. Results for the case when the splitter plate had been in position are shown arbitrarily at $z/d = -3$. The fact that they do not match the other results obtained at the same elevation ($z/d = -2.38$) shows that the effect of the free surface on the sectional force penetrated beyond this point—though it should be noted that the Reynolds number range is one where the loading is sensitive to small disturbances.

Elsewhere in Fig. 13 some distinct trends can be identified. Run-up on the front face of the cylinder produces finite drag coefficients at elevations above still water level. At a Froude number of 0.56, C_d is almost constant, but for Froude numbers between approximately 0.8 and 1.4, it increases with z at first, before falling to zero at the surface. This effect is strongest at $\mathrm{Fr} \approx 1$, when, at $z/d \approx -0.7$ the local drag coefficient reaches a maximum of more than twice its value at large submergences. When the Froude number is increased still further, the maximum in C_d becomes progressively less pronounced, and at $\mathrm{Fr} = 1.67$ has almost disappeared. It is clearly this increase in C_d just beneath the surface that is responsible for the peak in the total resistance coefficient that appears near $\mathrm{Fr} = 1$ in Figs. 5 and 6, and in Fig. 14 where the present results are shown. The latter were computed for the region $z/d > -2$, and show similar trends to those in Hay's data for the somewhat different case of a cylinder of draught $2d$ at about the same Reynolds numbers.

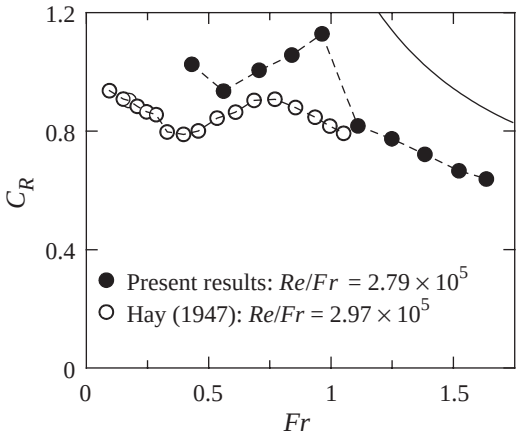

Fig. 14. Total resistance coefficients for $L/d = 2$. The present results refer to the region $-2d < z$ of a cylinder of much larger draught. In Hay's experiments the cylinder had a free end at $z = -2d$ with no endplate. A continuous line is $C_R = \frac{1}{2}(1 + 1/\mathrm{Fr}_L^2)$.

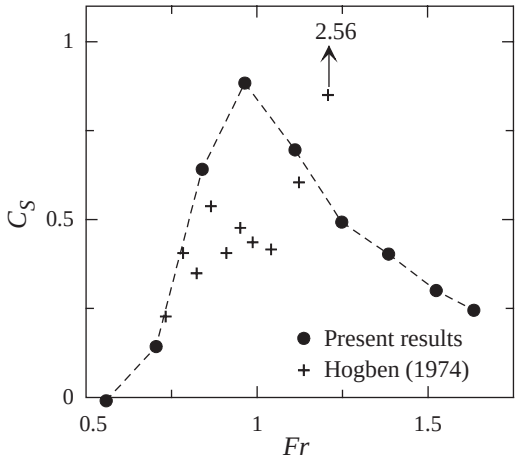

Fig. 15. Coefficient of surface resistance as a function of the Froude number.

From the distribution $C_d(z)$ for a given Froude number, the coefficient of surface resistance C_S can be found from Eqs. (1) to (4), adopting the drag coefficients plotted in Fig. 12 (and along the bottom axis in Fig. 13) as the corresponding C_{d0} in each case. The results are shown in Fig. 15, where C_S reaches a maximum of 0.9 at a Froude number close to 1. Except for two points near $Cs = 2.56$, Hogben's (1974) values of C_S are included, after having being multiplied by 25, as mentioned above.

If Hogben's idea of relating the resistance to that of a cylinder of elliptical cross-section were to be pursued, setting the ellipticity ε to 0.37 would achieve a peak value of C_S at the same Froude number of about 1. However, the corresponding ideal fluid wave resistance would then be about four times greater than that plotted in Fig. 15.

4.2. Pressure measurements

Measured stagnation and base pressures (at $\theta = 0^\circ$ and 180°) are plotted in Figs. 16 and 17 against elevations measured from still water level. At low Froude numbers, the stagnation pressures shown as heads of water h_{stag} in Fig. 16 match the distribution anticipated in Fig. 7(a), but at higher speeds the rate at which the pressure falls with increasing elevation is initially greater than that of a hydrostatic variation. In the upper part of the bow wave the reverse is true. The highest point at which pressures were measured was, in most cases, well below the elevation of the run-up observed in separate experiments (see below), and dashed lines in Fig. 16 join the points that represent the uppermost

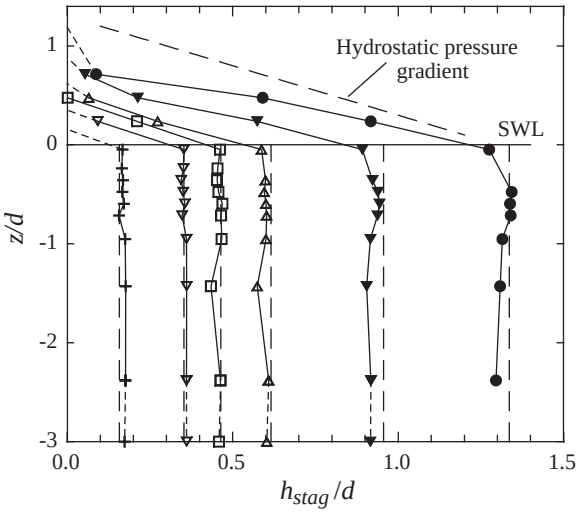

Fig. 16. Pressures on the centre-line of the upstream face of the cylinder at various Froude numbers identified by the symbols in Fig. 13. Long–dashed vertical lines represent $h_{stag}/d = \mathrm{Fr}^2/2$ for each case, and a sloping long–dashed line indicates the hydrostatic pressure gradient. Short–broken lines join the uppermost measurement at each Froude number to a point corresponding to zero pressure at the measured elevation of the run-up.

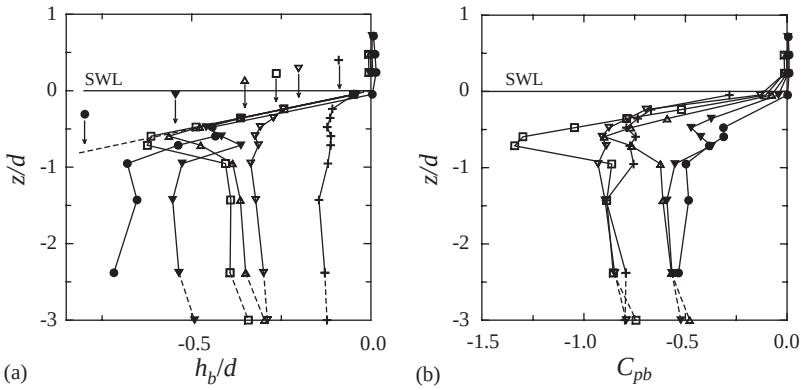

Fig. 17. Base pressures at various Froude numbers identified by the symbols in Fig. 13. In (a) the pressures are shown as heads of water, and the broken line represents the hydrostatic gradient. Symbols with arrows indicate the water surface elevations corresponding to $L_0/d = 0.286\mathrm{Fr}^2$. In (b) the same pressure data are plotted in the form of pressure coefficients.

pressure measurements to points at zero pressure at the elevation of the observed water surface. Since the flow in this region at the highest Froude numbers was highly aerated and probably not everywhere in contact with the cylinder (see Fig. 10), it is not surprising that the pressure gradient here should be less than hydrostatic. Similar departures from hydrostatic pressure gradients are found in hydraulic jumps at high Froude numbers (Rajaratnam, 1965).

Base pressures are similarly plotted in Fig. 17, both as heads of water h_b and as pressure coefficients $C_{pb} = 2gh_b/V^2$. At low Froude numbers the pressure distribution is similar to that sketched in Fig. 7(d), and as expected, in the ventilated region just below still water level the measurements follow a negative hydrostatic gradient identified in Fig. 17(a) by a dashed line which passes through the origin. As the Froude number is increased, a region of suction appears between one-half and one diameter beneath still water level, and this is clearly responsible for the increase in resistance at Froude numbers near 1 that is shown in Figs. 5, 6, 14 and 15.

The point at which each pressure distribution departs from the dashed line in Fig. 17(a) might be taken as an indication of the elevation of the water surface on the rear face of the cylinder. But except for the lowest two Froude numbers, the results of this assumption do not agree with Hay's measurements of the draw-down (Fig. 4) of $L_0/d = 0.286\mathrm{Fr}^2$. Points corresponding to this are indicated for each case by an arrow in Fig. 17(a). At a Froude

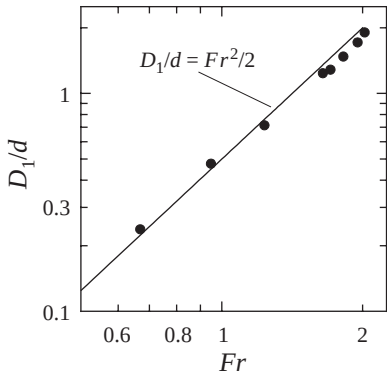

Fig. 18. Measurements of run-up on the front of the cylinder.

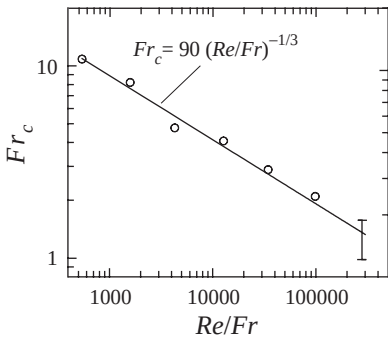

Fig. 19. The critical Froude number Fr_c, beyond which the run-up D_1 on the front of the cylinder no longer followed $D_1/d \propto \mathrm{Fr}^B$, as a function of Re/Fr. Open symbols are from Hay's (1947) data.

number of 0.96, the expected water surface elevation would be $z/d = -0.26$, but the pressure transducer at $z/d = -0.6$ appears to be exposed to atmospheric pressure. Also, the measurements in Fig. 17(a) suggest that the depression at $\mathrm{Fr} = 0.96$ is deeper than that at $\mathrm{Fr} = 1.38$. The difference may be due to the bubbly nature of the wake flow—as in the bow wave at high Froude numbers—or the presence of a cavity behind the cylinder that was not apparent in Hay's photographs.

4.3. Run-up

A few measurements of the maximum run-up on the front of the cylinder D_1 were made from video frames like that in Fig. 10, using a scale marked on the front of the cylinder. Results are plotted in Fig. 18 and suggest that the Froude number at which D_1/d first falls below $\mathrm{Fr}^2/2$ is between 1 and 1.6. This range is shown as a vertical line in Fig. 19, and can be seen to continue the trend found in Hay's results, where Fr_c is roughly proportional to $(\mathrm{Re}/\mathrm{Fr})^{-1/3}$.

5. Conclusions

New measurements of the resistance of a vertical surface-piercing circular cylinder of large draught in a steady current for a Reynolds number to Froude number ratio of 2.79×10^5 have shown that the total force coefficient reaches a maximum at a Froude number (based on the cylinder's diameter) of about 1. This is consistent with a reanalysis of the results of Hay (1947) (for the case of a cylinder with a submerged free end) and Hsieh (1964) (for cylinders standing on the floor of an open channel), and is found to be associated with a region of suction on the rear face of the cylinder that extends between one-half and one diameter beneath still water level, over a narrow range of Froude numbers.

The resistance due to the presence of the free surface was identified in the measurements as the difference between the total force and that which would arise if the form drag at large submergences were to extend, unchanged, from the base

of the cylinder up to the still water level. The corresponding coefficient of surface resistance (defined in Eq. (2)) reached a maximum value of about 0.9, suggesting that at a Froude number of about 1, the additional loading on a cylinder of large draught due to the free surface is comparable to the form drag on a length of cylinder of one diameter.

Hay's measurements of the run-up on the front face of the cylinder at a given Froude number reveal a strong dependence on the Reynolds number over the range $535 < \mathrm{Re}/\mathrm{Fr} < 9.83 \times 10^4$, and the present results are consistent with this trend. At the lowest Reynolds numbers, and for Froude numbers below a limiting value Fr_c, the run-up is almost proportional to the Froude number. As Re/Fr is increased, the relationship becomes progressively more nonlinear, until, when Re/Fr is greater than about 10^4, it becomes a quadratic one in agreement with Bernoulli's equation for inviscid flow. The limiting value Fr_c is roughly proportional to $(\mathrm{Re}/\mathrm{Fr})^{-1/3}$, falling from 11 at $\mathrm{Re}/\mathrm{Fr} = 535$ to less than 1.6 at $\mathrm{Re}/\mathrm{Fr} = 2.79 \times 10^5$. Pressure measurements on the rear face of the cylinder reveal the extent of the ventilated region, which seems not to grow monotonically with increasing Froude number.

Acknowledgements

This work was supported by EPSRC under Grant GR/L69879, and by Statoil.

References

Farivar, D., 1981. Turbulent uniform flow around cylinders of finite length. American Institute of Aeronautics and Astronautics Journal 19, 275–281.

Goldstein, S. (Ed.), 1965. Modern Developments in Fluid Dynamics, Vol. 2. Dover Publications, New York, p. 439.

Hay, A.D., 1947. Flow about semi-submerged cylinders of finite length. Princeton University Report, Princeton, NJ.

Hoerner, S.F., 1956. Hydrodynamic Drag. Published by the author.

Hogben, N., 1974. Wave resistance of surface piercing vertical cylinders in uniform currents. NPL Report Ship 183.

Hogben, N., Standing, R.G., 1975. Wave pattern resistance from routine model tests. Transactions of the Royal Institution of Naval Architects, 279–300 (issued for written discussion as paper W11 1974).

Hsieh, T., 1964. Resistance of cylindrical piers in open channel flow. Journal of the Hydraulics Division, Proceedings of the American Society of Civil Engineers 90, 161–173.

Inoue, M., Baba, N., Himeno, Y., 1993. Experimental and numerical study of viscous flow field around an advancing vertical circular cylinder piercing a free surface. Journal of the Kansai Society of Naval Architects of Japan 220, 57–64 (in Japanese).

Kotik, J., Morgan, R., 1969. The uniqueness problems for wave resistance calculated from singularity distributions which are exact at zero Froude number. Journal of Ship Research 13, 61–68.

Newman, J.N., 1977. Marine Hydrodynamics. The MIT Press, Cambridge, MA.

Rajaratnam, N., 1965. The hydraulic jump as a wall jet. Proceedings of the American Society of Civil Engineers. Journal of the Hydraulics Division 91, 107–132.

Yeung, R.W., Yu, X., 2001. Three-dimensional free-surface flow with viscosity: a spectral solution. In: Kashiwagi, M. (Ed.), Hydrodynamics in Ship and Ocean Engineering. Research Institute for Applied Mechanics. Kyushu University, Kyoto, pp. 87–114.

Younis, B.A., Teigen, P., Przulj, V.P., 2001. Estimating the hydrodynamic forces on a mini TLP with computational fluid dynamics and design-code techniques. Ocean Engineering 28, 585–602.

Zdravkovich, M.M., 1997. Flow Around a Circular Cylinder. Oxford University Press, Oxford